

Enhanced Photoelectrochemistry in Supramolecular CdS-Nanoparticle-Stoppered Pseudorotaxane Monolayers Assembled on Electrodes

Laila Sheeney-Haj-Ichia and Itamar Willner*

Institute of Chemistry, The Farkas Center for Light Induced Processes, The Hebrew University of Jerusalem, Jerusalem 91904, Israel

Received: September 19, 2002

A pseudorotaxane monolayer consisting of a supramolecular complex generated between cyclo-bis(paraquat-*p*-phenylene), (**1**), and the 1,4-bis(mercapto ethyloxy ethyloxy ethyl)benzene monolayer, (**2**), that is stoppered by CdS nanoparticles (3–5 nm) is generated on Au electrodes. The surface coverage of the supramolecular complex units and the associated CdS particles corresponds to $2.4 \pm 0.2 \times 10^{-10}$ mole·cm⁻² and 3×10^{12} particles·cm⁻², respectively. The photocurrent generated by the (**1**)/(**2**)-CdS pseudorotaxane architecture is 8-fold higher than in a CdS-nanoparticle monolayer system that lacks (**1**). The enhanced photocurrent in the pseudorotaxane assembly is attributed to vectorial electron transfer of photoexcited conduction-band electrons to the threaded electron acceptor (**1**), which leads to charge separation and to the retardation of the electron–hole recombination process.

The assembly of semiconductor nanoparticles in monolayer and thin film systems attracts substantial research efforts directed to the development of photoelectrochemical systems,^{1,2} light emitting diodes,³ and sensor devices.⁴ For enhanced photocurrent generation, the retardation of the recombination of the photo-generated electron–hole pair is essential. The use of molecular cross-linked semiconductor nanoparticles of controlled chemical composition⁵ and the application of core–shell hybrid systems of different semiconductor materials⁶ were reported to facilitate charge separation and enhance photocurrent generation. For example, a bifunctional nanoporous film consisting of CdS/SnO₂ reveals improved photoelectrochemical features due to vectorial electron transfer of conduction-band electrons from CdS to the conduction band of SnO₂, resulting in the electron–hole separation in the two particles. Recently, we reported on the assembly of covalently linked bipyridinium semiconductor nanoparticles on electrode supports for enhanced photocurrent generation.⁷ Vectorial electron transfer of photogenerated conduction-band electrons to the bipyridinium relay units led to spatial charge separation and increased photocurrents.

The tailoring of noncovalent supramolecular architectures on surfaces is a rapidly developing research area. Threaded catenane architectures in monolayer structures,⁸ molecular mechanical translocation in stoppered rotaxane configurations,⁹ and layered receptor- and photosensitizer-relay cross-linked Au nanoparticles were reported for sensory¹⁰ and photoelectrochemical¹¹ applications. Here we report on the assembly of a pseudorotaxane monolayer assembly consisting of a CdS-nanoparticle-stoppered system of cyclo-bis(paraquat-*p*-phenylene), (**1**), that is threaded on a 1,4-bis(mercapto ethyloxy ethyloxy ethyl)benzene monolayer, (**2**). To our knowledge, this is the first example of a nanoparticle-stoppered pseudorotaxane assembly on a surface. In addition to the enhanced photocurrents observed in the nanoarchitected monolayer, the concept may be broadened to tailor new supramolecular electronic and optoelectronic systems in monolayer and thin film configurations.

Experimental Section

Microgravimetric Quartz Crystal Microbalance (QCM) Measurements. Experiments were performed with a QCM analyzer (Fluke) using Au–quartz crystals (AT-cut 10 MHz). The geometrical area of the Au electrode was 0.20 ± 0.05 cm². Prior to each measurement the modified QCM crystals were dried under a flow of argon, and the crystal frequencies were determined in air. The surface coverage of the respective components was determined by following the frequency change of the crystals upon the stepwise assembly of the different components. The surface coverage was estimated using the Sauerbrey equation¹² (eq 1), where Δm is the mass change, f_0 is the resonance frequency of the quartz crystal, A is the piezoelectrically active area, ρ_q is the density of quartz (2.648 g·cm⁻³), and μ_q is the shear modulus (2.947×10^{11} dyn·cm⁻³ for AT-cut quartz).

$$\Delta f = -2f_0^2 \frac{\Delta m}{A(\mu_q \rho_q)^{1/2}} \quad (1)$$

Photoelectrochemical Measurements. Photoelectrochemical experiments were performed using a home-built photoelectrochemical system that included a 300 W Xe lamp (Oriel, model 6258), a monochromator (Oriel, model 74000), and a chopper (Oriel, model 76994). The electrical output from the cell was sampled by a lock-in amplifier (Stanford Research model SR 830 DSP). The shutter chopping frequency was controlled by a Stanford Research pulse/delay generator model DE 535. The photoelectrode consisted of the CdS-nanoparticle-stoppered pseudorotaxane assembled on the Au–quartz crystal or the CdS nanoparticle-functionalized electrode. A graphite electrode was used as a counter electrode. The photogenerated current was measured between the working and counter electrode. The electrolyte solution consisted of 0.02 M triethanolamine in 0.1 M phosphate buffer, pH 9.5.

Electrochemical Measurements. Cyclic voltammetry was performed in a standard electrochemical cell using the func-

* Corresponding author. E-mail: willnea@vms.huji.ac.il.

tionalized Au–quartz crystals. A conventional three-electrode cell, consisting of the Au–quartz electrode, a glassy carbon auxiliary electrode isolated by a glass frit and a saturated calomel electrode (SCE) connected to the working volume with a luggin capillary, was used for the electrochemical measurements. The potentials measured upon cyclic voltammetry are reported vs the SCE. The cell was positioned in a grounded Faraday cage. Cyclic voltammetry was performed using a potentiostat (EG&G, model 283) connected to the computer (EG&G Software Power Suite 1.03). All electrochemical measurements were performed in 0.1 M sodium borate (pH = 9.2) as background electrolyte.

Materials. All materials were obtained from Aldrich. Cyclo-bis(paraquat-*p*-phenylene)tetrahexafluorophosphate was synthesized according to the literature.¹³

Synthesis of 1,4-Bis(mercapto ethyl oxyethyl oxyethyl)benzene. Triethylene glycol di-*p*-tosylate (12 g, 24 mmol) and *p*-hydroquinone (1.5 g, 13 mmol) were dissolved in a suspension of K₂CO₃ (15 g, 100 mmol) in dry MeCN (150 mL). The mixture was flushed with Ar, then was stirred under Ar at reflux for 7 days. The resulting reaction mixture was cooled, filtered, and the solid was washed with MeCN (20 mL). The solvent was removed under vacuum, giving a crude residue that was purified by column chromatography (9:1 dichloromethane/ethyl acetate on silica gel) to give pure 1,4-bis(tosylate ethyloxy ethyloxy ethyl)benzene (2 g, 46%). NMR spectra in CDCl₃, ¹H: δ (ppm) 1.66 (s, 6H), 3.5–4.1 (m, 24H), 6.82 (s, 4H), 7.2 (d, 4H), 7.8 (d, 4H).

1,4-Bis(tosylate ethyl oxyethyl oxyethyl)benzene (2 g, 5.5 mmol) and thioacetate (9.4 g, 82 mmol) were dissolved in dry DMF (100 mL). The mixture was flushed with Ar, then stirred under Ar at room temperature for 7 days. The solvent was removed under vacuum, yielding a crude product which was dissolved in dichloromethane and washed twice with H₂O. The organic phase was dried to yield 1,4-bis(thioacetate ethyl oxyethyl oxyethyl)benzene (1 g). ¹H NMR spectra in CDCl₃: δ (ppm) 1.6 (s, 6H), 3.1 (t, 24H), 3.5–3.65 (m, 12H), 3.83 (t, 4H), 4.08 (t, 4H), 6.8 (s, 4H).

1,4-Bis(thioacetate ethyl oxyethyl oxyethyl)benzene (1 g, 2 mmol) was added to 20 mL sodium methoxide solution (15 mg sodium/mL methanol). After standing for 5 min the solvent was removed under vacuum at 20 °C, giving a crude product which was dissolved in dichloromethane that was washed with 10% NaOH. After a second extraction of the dichloromethane solution with 10% NaOH, the solutions were combined and the organic phase was discarded. The aqueous layer was acidified with cold 10% H₂SO₄, the product was extracted into dichloromethane (3× extractions). The combined dichloromethane solution was dried over Na₂SO₄, filtered, and evaporated to give pure 1,4-bis(mercapto ethyloxy ethyloxy ethyl)benzene. ¹H NMR: δ (ppm) 2.5 (t, 4H), 2.9 (t, 4H), 3.43–3.7 (m, 12H), 4.00 (t, 4H), 6.85 (s, 4H).

Preparation of CdS Nanoparticles.¹⁴ An AOT/*n*-heptane water-in-oil micromulsion was prepared by the solubilization of 2 mL distilled water in 100 mL *n*-heptane in the presence of 7.0 g of the AOT surfactant (dioctyl sulfosuccinate, sodium salt). The resulting mixture was separated into 60 mL and 40 mL of reverse-micelle subvolumes. Aqueous solutions of Cd(ClO₄)₂ (0.24 mL, 1 M) and Na₂S (0.16 mL, 1 M) were added to the 60 mL and 40 mL subvolumes, respectively, and allowed to stir for 1 h. The two solutions were united and stirred under argon for 1 h to yield the nanoparticles. The resulting mixture was stirred for 24 h.

Preparation of CdS-Nanoparticle-Stoppered Pseudorotaxane Monolayer. The Au–quartz crystals were modified with 1,4-

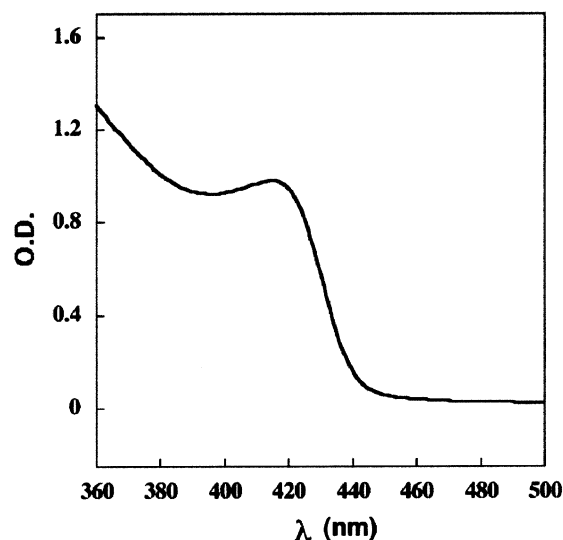


Figure 1. Absorption spectrum of AOT-capped CdS nanoparticles (diameter 3–5 nm).

bis(mercapto ethyloxy ethyloxy ethyl)benzene monolayer (0.02 M in DMSO for 2 h). The functionalized electrodes were treated for 2 h with 2 mL of a solution of cyclo-bis(paraquat-*p*-phenylene)tetrahexafluorophosphate in acetone, 0.02 M, followed by the addition of 2 mL of the suspension of CdS nanoparticles in the reversed micelles. The Au–quartz crystals were allowed to interact with the CdS nanoparticles for 12 h. The resulting electrodes were washed with 0.05 sodium chloride solution.

Results and Discussion

CdS nanoparticles (3–5 nm diameter determined by TEM) were prepared according to the literature in an AOT (dioctyl-sulfosuccinate, Na⁺)/heptane/H₂O reverse micellar system.¹⁴ The absorption spectrum of the capped CdS nanoparticles is shown in Figure 1.

1,4-Bis(mercapto ethyloxy ethyloxy ethyl)benzene, (**2**), was synthesized according to the details given in the Experimental Section. To characterize the composition of the CdS-stoppered pseudorotaxane, the system was assembled on an Au–quartz piezoelectric crystal (AT-cut, 10 MHz), Scheme 1(A). The dithiol (**2**) was assembled on the Au surface of the Au–quartz crystal. From the change in the crystal frequency, $\Delta f = -90$ Hz, we estimate the surface coverage to be 2.8×10^{-10} mole·cm⁻². The resulting monolayer was then interacted with the bis-bipyridinium cyclophane, (**1**). The π -donor dialkoxybenzene unit in (**2**) forms a labile acceptor–donor complex on the Au surface. To the equilibrated system, the CdS nanoparticles in the reverse micellar system were added to yield the stoppered pseudorotaxane. A related reference system was generated by the linkage of the CdS nanoparticles to the (**2**)-functionalized monolayer in the absence of (**1**), Scheme 1B. From the changes in the crystal frequencies upon the assembly of the two systems, $\Delta f = -395$ Hz for configuration A and $\Delta f = -296$ Hz for configuration B, we estimate the surface coverage of the CdS nanoparticles to be 3×10^{12} particles·cm⁻² and the surface coverage of the threaded (**1**) to be $2.4 \pm 0.2 \times 10^{-10}$ mole·cm⁻². Thus, ca. 48 pseudorotaxane units are stoppered by each CdS nanoparticle.

Figure 2, curve (a), shows the cyclic voltammograms of the CdS-stoppered (**1**)-pseudorotaxane that reveals the characteristic quasi-reversible redox wave of (**1**). Coulometric assay of the reduction (or oxidation) wave of (**1**) indicates a surface coverage

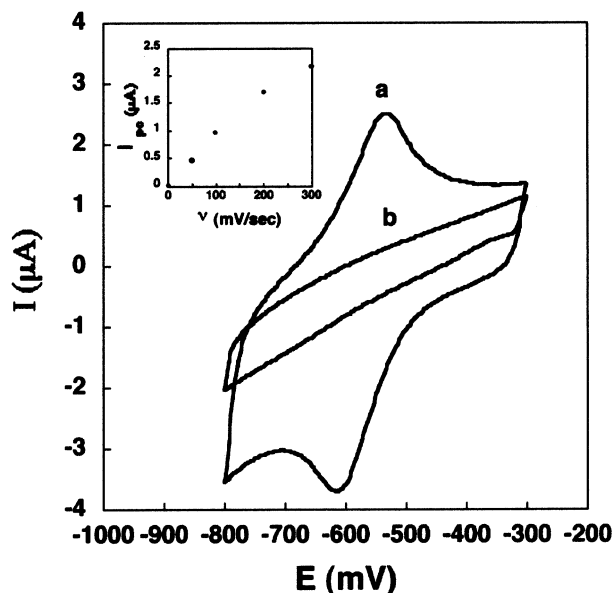


Figure 2. Cyclic voltammetry of (a) CdS-stoppered (**1**) pseudorotaxane monolayer-functionalized Au-quartz crystal. (b) CdS-nanoparticle monolayer-functionalized Au-quartz crystal. Data recorded in 0.1 M sodium borate solution, pH = 9.2 under Ar, scan rate $100 \text{ mV}\cdot\text{s}^{-1}$. Inset: Cathodic peak current of (**1**) at different scan rates.

of $2.0 \pm 0.2 \times 10^{-10} \text{ mole}\cdot\text{cm}^{-2}$, consistent with the value extracted from the microgravimetric quartz crystal microbalance experiments. The peak current of the redox-wave of (**1**) relates directly to the scan rate (cf. Figure 2, inset), consistent with a surface-confined configuration of (**1**). Figure 2, curve (b), shows the cyclic voltammogram of the CdS-nanoparticle monolayer linked to the electrode surface with the dithiol wire (**2**). The latter configuration was treated with (**1**). As the CdS nanoparticles are capped with a negatively charged protecting monolayer of AOT surfactant, the electrostatic binding of (**1**) to the particles may occur. Indeed, we find that (**1**) associates with the CdS nanoparticles by electrostatic interactions, but the surface-bound (**1**) is completely washed-off with 0.05 M sodium chloride solution. In contrast, the (**1**)-pseudorotaxane configuration is not affected when rinsing the system with the sodium chloride solution. This result further confirms that a supramolecular CdS-stoppered rotaxane is generated on the electrode.

SCHEME 1: (A) Assembly of the Pseudorotaxane Monolayer Consisting of CdS Nanoparticles on Au-Quartz Crystal; (B) Assembly of the CdS-Nanoparticle Monolayer on the Au-Quartz Crystal in the Absence of (**1**)

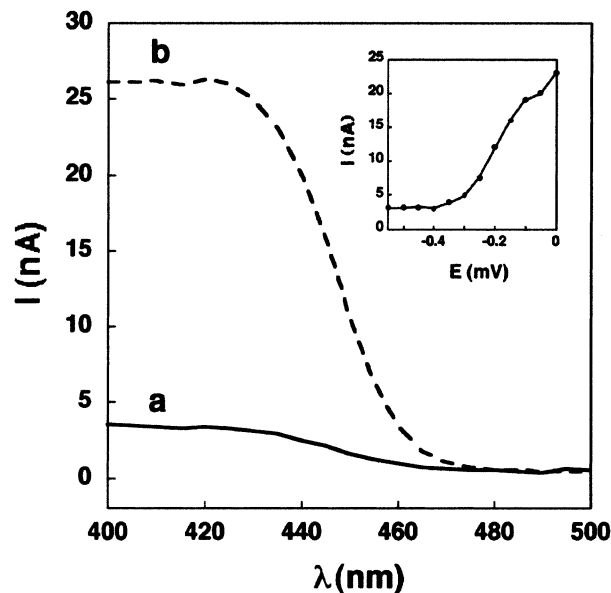
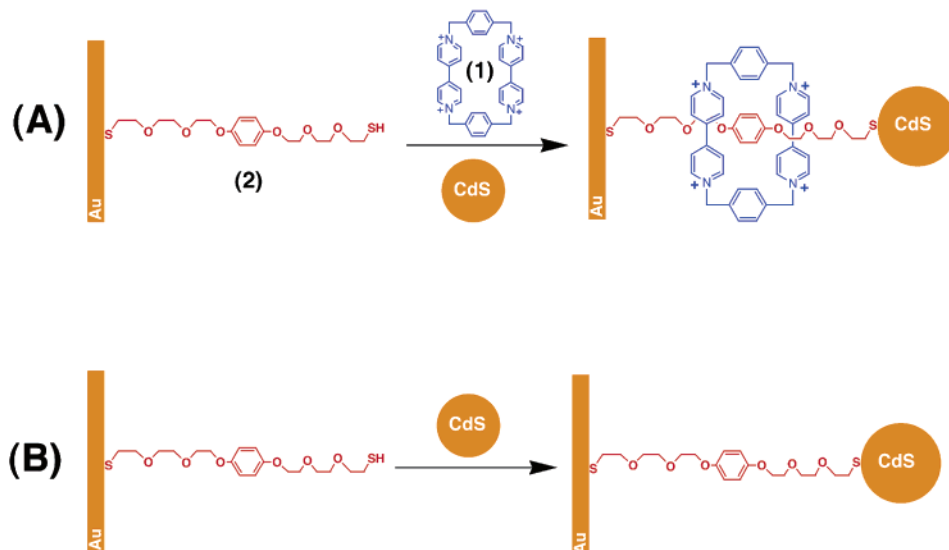


Figure 3. Photocurrent spectra of nanoparticle-functionalized Au-quartz crystals: (a) CdS-nanoparticle monolayer; (b) CdS-nanoparticle-stoppered (**1**) pseudorotaxane system. Data recorded in phosphate buffer solution 0.1 M, pH = 9.5, that included triethanolamine, $2 \times 10^{-2} \text{ M}$. Electrodes are biased at $E = 0.0 \text{ V}$ vs SCE. Inset: Photocurrents (upon irradiation at 420 nm) as a function of applied potential on the electrode.

Figure 3, curve (a), shows the photocurrent spectrum observed upon illumination of the CdS-monolayer electrode without (**1**), whereas curve (b) shows the photocurrent action spectrum resulting in the irradiation of the supramolecular (**1**)-pseudorotaxane CdS system. Clearly, the photocurrent generated in the latter system is ca. 8-fold higher than the photocurrent observed in the CdS monolayer only. The photocurrent action spectrum follows the absorbance band of the CdS nanoparticles ($\lambda_{\text{max}} = 420 \text{ nm}$), indicating that it originates from the photoexcitation of the nanoparticles. The light-to-current conversion quantum efficiency in the (**1**)-pseudorotaxane-CdS system corresponds to $\phi = 1.55\%$. The enhanced photocurrent observed in the presence of the (**1**)-pseudorotaxane system is attributed to vectorial electron transfer in the system that yields charge separation, retardation of recombination processes, and

efficient electron transfer to the electrode. In the assembly consisting of CdS nanoparticles without (**1**), rapid electron–hole recombination perturbs electron ejection into the electrode and the generation of the photocurrent. On the other hand, in the supramolecular assembly, the transfer of the conduction-band electron to the threaded relay, (**1**), leads to spatial charge separation and the retardation of the back electron transfer. Subsequent electron transfer from the reduced relay to the electrode leads to the effective generation of the photocurrent. This explanation is supported by the fact that application of a potential on the electrode that reduces (**1**) to the respective radical cation, $E = -0.55$ vs SCE, blocks the effective photocurrent generation. That is, reduction of (**1**) perturbs the relay functions of the threaded element, Figure 3, inset.

In conclusion, we have described a novel approach to assemble supramolecular pseudorotaxane–CdS-nanoparticle architectures on surfaces for enhanced photocurrent generation. Vectorial electron transfer in the system, which results in charge separation, leads to the improved photoelectrochemical functions of the system.

Acknowledgment. This research is supported by the Enrique Berman Fund, The Hebrew University of Jerusalem.

References and Notes

- (1) Alivisatos, A. P. *Science* **1996**, *271*, 933–937.
- (2) Klein, D. L.; Roth, R.; Lim, A. K. L.; Alivisatos, A. P.; McEuen, P. L. *Nature* **1997**, *389*, 699–701.
- (3) Tessler, N.; Medvedev, V.; Kazes, M.; Kan, S. H.; Banin, U. *Science* **2002**, *295*, 1506–1508.
- (4) Willner, I.; Patolsky, F.; Wasserman, J. *Angew. Chem., Int. Ed.* **2001**, *40*, 1861–1864.
- (5) Nasr, C.; Hotchandani, S.; Kim, W. Y.; Schmehl, R. H.; Kamat, P. V. *J. Phys. Chem. B* **1997**, *101*, 7480–7487.
- (6) Zaban, A.; Chen, S. G.; Chappel, S.; Gregg, B. A. *Chem. Commun.* **2000**, 2231–2232.
- (7) Sheeney-Haj-Ichia, L.; Wasserman, J.; Willner, I. *Adv. Mater.* **2002**, *14*, 1323–1326.
- (8) (a) Lu, T. B.; Zhang, L.; Gokel, G. W.; Kaifer, A. E. *J. Am. Chem. Soc.* **1993**, *115*, 2542–2543. (b) Nadai, C. De.; Whelan, C. M.; Perollier, C.; Clarkson, G.; Leigh, D. A.; Caudano, R.; Rudolf, P. *Surf. Sci.* **2000**, *454*, 112–117. (c) Collier, C. P.; Jeppesen, J. O.; Luo, Y.; Perkins, J.; Wong, E. W.; Heath, J. R.; Stoddart, J. F. *J. Am. Chem. Soc.* **2001**, *123*, 12632–12641.
- (9) (a) Luo, Y.; Collier, C. P.; Jeppesen, J. O.; Nielslen, K. A.; Delonno, E.; Ho, G.; Perkins, J.; Tseng, H.-R.; Yamamoto, T.; Stoddart, J. F.; Heath, J. R. *ChemPhysChem* **2002**, *3*, 519–525. (b) Pease, A. R.; Jeppesen, J. O.; Stoddart, J. F.; Luo, Y.; Collier, C. P.; Heath, J. R. *Acc. Chem. Res.* **2001**, *34*, 433–444. (c) Willner, I.; Pardo-Yissar, V.; Katz, E.; Ranjit, K. T. *J. Electroanal. Chem.* **2001**, *497*, 172–177.
- (10) (a) Lahav, M.; Shipway, A. N.; Willner, I. *J. Chem. Soc., Perkin Trans. 2* **1999**, 1925–1931. (b) Lahav, M.; Gabai, R.; Shipway, A. N.; Willner, I. *Chem. Commun.* **1999**, 1937–1938.
- (11) (a) Lahav, M.; Gabriel, T.; Shipway, A. N.; Willner, I. *J. Am. Chem. Soc.* **1999**, *121*, 258–259. (b) Lahav, M.; Heleg-Shabtai, V.; Wasserman, J.; Katz, E.; Willner, I.; Dürr, H.; Hu, Y. Z.; Bossmann, S. H. *J. Am. Chem. Soc.* **2000**, *122*, 11480–11487.
- (12) Athey D.; Ball, M.; McNeil, C. J.; Armstrong, R. D. *Electroanalysis* **1995**, *7*, 270.
- (13) (a) Odell, B.; Reddington, M. V.; Slawin, A. M. Z.; Spencer, N.; Stoddart, J. F. *Angew. Chem., Int. Ed. Engl.* **1988**, *27*, 1547–1550. (b) Asakawa, M.; Dehcan, W.; L'Abbé, G.; Menzer, S.; Nouwen, J.; Raymo, F. M.; Stoddart, J. F.; Williams, D. J. *J. Org. Chem.* **1996**, *61*, 9591–9595.
- (14) Steigenwald, M. L.; Alivisatos, A. P.; Gibson, J. M.; Harris, T. D.; Kortan, R.; Muller, A. J.; Thayer, A. M.; Duncan, T. M.; Douglass, D. C.; Brus, L. E. *J. Am. Chem. Soc.* **1988**, *110*, 3046–3050.